Ultramicroscopy 169 (2016) 80–88

Contents lists available at ScienceDirect

Ultramicroscopy

journal homepage: www.elsevier.com/locate/ultramic

Photogrammetry of the three-dimensional shape and texture of a nanoscale particle using scanning electron microscopy and free software

Lionel C. Gontard [a,b,*], Roland Schierholz [c], Shicheng Yu [c], Jesús Cintas [d], Rafal E. Dunin-Borkowski [e]

[a] Departamento de Ciencia de los Materiales e Ingeniería Metalúrgica y Química Inorgánica, Universidad de Cádiz, Puerto Real 11510, Spain
[b] Faico PCT Cartuja. Edif. TI Marie Curie, C/ Leonardo da Vinci 18, 4ª Planta, 41092 Sevilla, Spain
[c] Institute of Energy and Climate Research, Fundamental Electrochemistry (IEK-9), Forschungszentrum Jülich, D-52425 Jülich, Germany
[d] Servicio de Microscopía Centro de Investigación, Tecnología e Innovación (CITIUS), Universidad de Sevilla, Av. Reina Mercedes 4b, 41012 Sevilla, Spain
[e] Ernst Ruska-Centre for Microscopy and Spectroscopy with Electrons and Peter Grünberg Institute, Forschungszentrum Jülich, D-52425 Jülich, Germany

ARTICLE INFO

Article history:
Received 10 April 2016
Received in revised form
28 June 2016
Accepted 3 July 2016
Available online 6 July 2016

Keywords:
Three-dimensional scanning electron microscopy
Photogrammetry
Surface texture
Image processing
Freeware
Nanoscale particle morphology
$LiTi_2(PO_4)_3$

ABSTRACT

We apply photogrammetry in a scanning electron microscope (SEM) to study the three-dimensional shape and surface texture of a nanoscale $LiTi_2(PO_4)_3$ particle. We highlight the fact that the technique can be applied non-invasively in any SEM using free software (freeware) and does not require special sample preparation. Three-dimensional information is obtained in the form of a surface mesh, with the texture of the sample stored as a separate two-dimensional image (referred to as a UV Map). The mesh can be used to measure parameters such as surface area, volume, moment of inertia and center of mass, while the UV map can be used to study the surface texture using conventional image processing techniques. We also illustrate the use of 3D printing to visualize the reconstructed model.

1. Introduction

Several different techniques are available for the three-dimensional (3D) characterization of micro- and nano-scale structures using electrons. In the transmission electron microscope (TEM), electron tomography [7,14,21,23,37] and single particle reconstruction [27] can be applied to studies of thin samples. In the scanning electron microscope (SEM), scanning TEM (STEM) tomography can be used to study very thin samples [12,15,20,30], while for sample dimensions of between μm and mm an ensemble of techniques based on the destructive *slice and view* approach has been developed [2,9,26,29,33]. In contrast, for studies of sample surfaces in three dimensions, non-destructive techniques based on photogrammetry can be applied, albeit at the cost of not reconstructing the inner volume of the sample. For example, stereophotogrammetry can be used to obtain three-dimensional topographic reconstructions, typically from two images recorded in the form of a stereo pair [28,31,34,38]. The technique is used extensively in metrological applications [3,5,6,16].

Here, we illustrate a methodology for the high spatial resolution 3D reconstruction of surfaces and textures in the SEM using photogrammetry, a technique that has been applied routinely in scientific fields such as geology [11] and reviewed by Bemis et al. [4]. Although the final spatial resolution and fidelity that can be achieved using this type of reconstruction depends on the aberrations of the electron beam, the contrast mechanism used to record the images, the details of the particular sample and the magnification used, the technique, which involves the acquisition of a series of images of the sample from different perspectives, can be applied in any SEM so long as the sample can be tilted with respect to the electron beam. In SEM, Eulitz and Reiss [10] recently described the principle of the method and used it to reconstruct a 3D model of a rabbit kidney glomerulus from SEM images, although they did not attempt to perform any quantitative analysis of the final 3D model.

In order to demonstrate the applicability of the technique and discuss its advantages and limitations, we use it to study a particle

* Corresponding author at: Departamento de Ciencia de los Materiales e Ingeniería Metalúrgica y Química Inorgánica, Universidad de Cádiz, Puerto Real 11510, Spain.
E-mail address: lionelcg@gmail.com (L.C. Gontard).
URL: http://www.lcgontard.es (L.C. Gontard).

http://dx.doi.org/10.1016/j.ultramic.2016.07.006
0304-3991/

of $LiTi_2(PO_4)_3$ [36] using a secondary electron (SE) signal in an SEM. This material has applications in Li ion flow batteries, which have a high energy density and in which the charge carrier is in the form of grains suspended in liquid. We show that quantitative analysis of the shape and surface of the 3D model is possible with little effort using open-source software. Moreover, the texture of the 3D model, which is accessible in a so-called UV map (see below), can be used to measure surface properties, such as the size distribution of nanoparticles segregated outside a primary particle.

2. Results and discussion

Fig. 1 shows representative experimental images of a $LiTi_2(PO_4)_3$ particle taken from a series of 37 images recorded at 2 kV using an SE detector in an SEM. The images were each recorded with a size of 1337 × 1000 pixels using the following procedure: (1) the pin mount in the SEM was moved to an α-tilt angle of 52° and 18 images were recorded by rotating the sample in steps of 20°. At this high tilt angle, details of the sample close to the substrate could be recorded; (2) the sample tilt was changed to an α-tilt angle of 32° and 17 images were recorded in steps of 20° (3) a final image was recorded at an α-tilt angle of 0°.

Algorithms for photogrammetry typically attempt to perform what is known as "bundle adjustment". Given a set of images that depicts a number of 3D points from different viewpoints, bundle adjustment is based on the simultaneous refinement of the 3D coordinates that describe the geometry of the scene and the parameters that describe its relative motion, according to an optimization criterion that involves the evaluation of corresponding image projections of all points.

The requirements for successful 3D reconstruction include rigidity of the sample and sufficient textural details so that consecutive images can be stitched together and so that dense correspondence maps can be linked together over different viewpoints. (A dense correspondance map is a 3D point cloud that is converted into a triangular mesh). The mesh can be texture-mapped to achieve a photo-realistic appearance.

We attempted to use two freeware programs that are available for photogrammetric reconstruction. We first applied *VisualSFM*

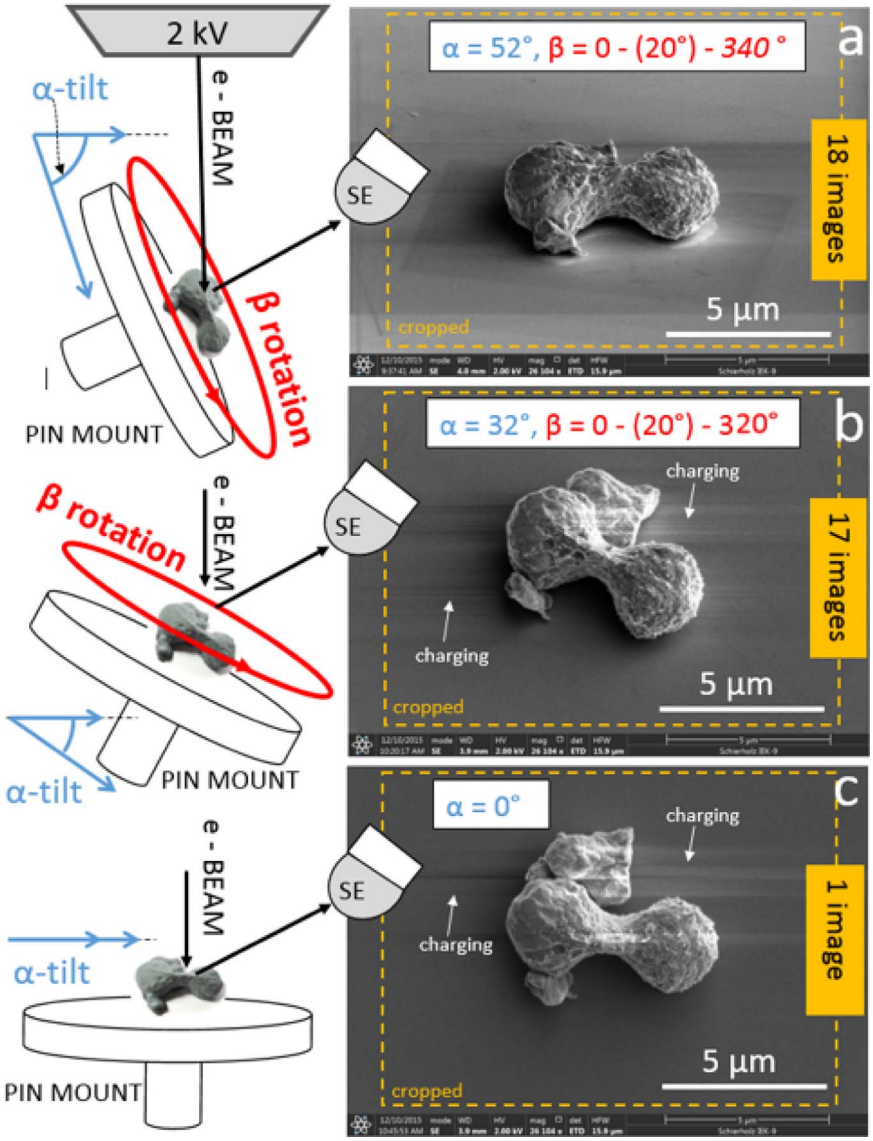

Fig. 1. Illustration of the acquisition of images for reconstruction using photogrammetry. In the present study, three sets of images of a $LiTi_2(PO_4)_3$ particle were recorded at different α-tilt angles: (a) At $\alpha = 52°$, 18 images were recorded in in-plane rotation steps of 20°. (b) At $\alpha = 32°$, 17 images were recorded in in-plane rotation steps of 20°. (c) At $\alpha = 0°$, one image was recorded looking down onto the sample. For further processing, the 36 images were cropped to the dimensions marked by the dashed squares in (a–c). The images show streaks due to electrostatic charging of the sample (marked using white arrows).

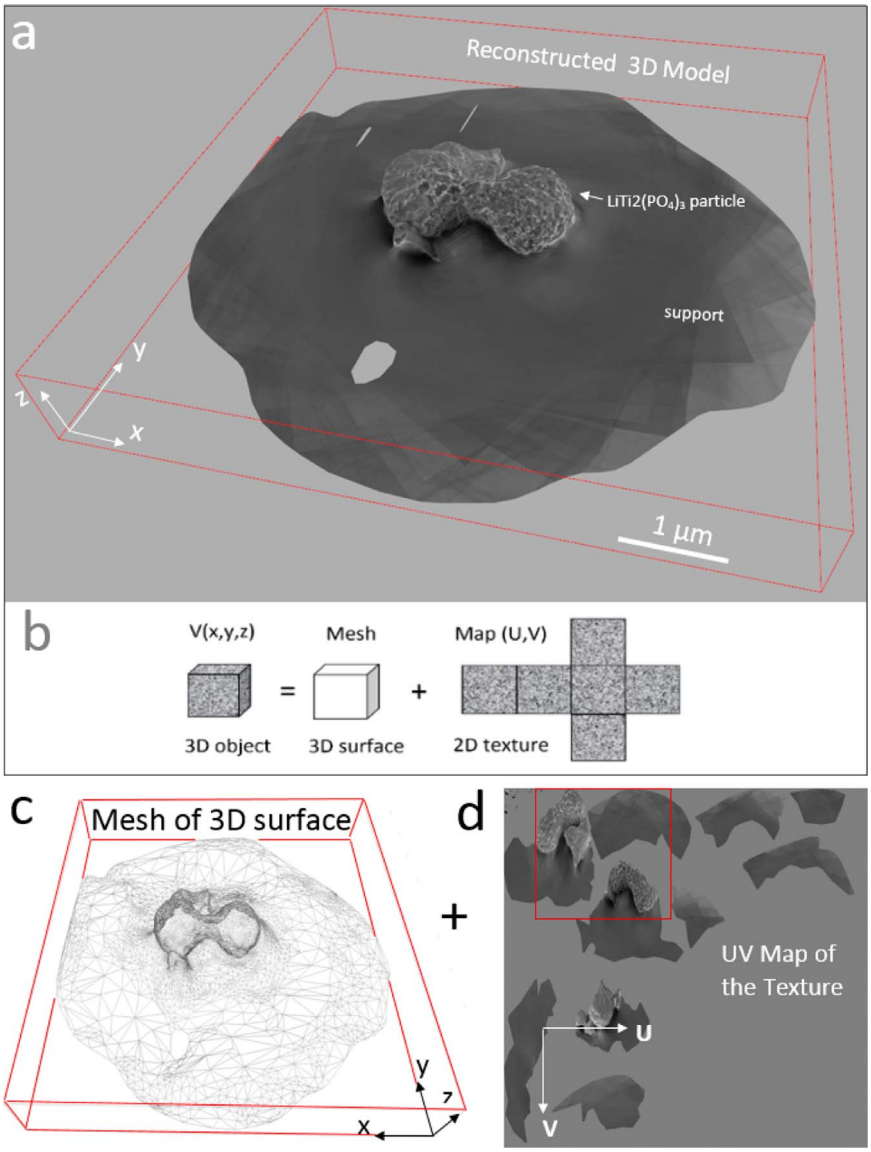

Fig. 2. (a) Visualization of the reconstructed 3D model of a $LiTi_2(PO_4)_3$ particle. (b) Schematic illustration of the fact that the model consists of a 3D surface mesh wrapped by a two-dimensional texture. (c) 3D surface mesh with 11,793 faces and 5952 vertices. (d) Texture displayed in the form of a two-dimensional UV map. Each triangle in the 3D mesh is rearranged onto the texture map by assigning two coordinates, U and V. The marked area in the UV map was used for the PSD measurements shown in Fig. 4.

[35], an offline application that performs a point cloud reconstruction that must then be converted into a mesh. However, the software failed when it was applied to the present dataset. We then applied *123D Catch* [1] photogrammetry software from *Autodesk*, which can be downloaded locally onto a PC but the reconstruction is then performed online. By using this program, we succeeded in obtaining a 3D model of the $LiTi_2(PO_4)_3$ particle, which is shown in Fig. 2. The reconstruction was obtained without making use of any prior information about the sample, its orientation or the imaging parameters.

The number of images and the range of sample tilt angles that must be used for photogrammetric reconstruction must be high enough to achieve correct stitching between successive images and complete reconstruction of the sample. In particular, high sample tilt angles are needed to record details close to the support, which can be obscured by the sample itself at lower tilt angles.

Because photogrammetry software performs stitching of successive images based on their intensities, they must include overlapping regions. In addition, surfaces that are featureless or contain regular patterns should be avoided. When *123D Catch* software [1] is used, the optimal number of images is greater than 50, distributed over one or more tilt angles. The maximum number of images accepted by the software is 70. The images should be acquired with an overlap of up to 50%. As a rule of thumb, the same details of an area of the sample should be contained in 3 or 4 different images. A valid image sequence can be acquired with an angular step of approximately 20° between successive images. If the sample contains small occlusions (i.e., details that are not accessible in any image), then the angular step between images should be decreased to 5–10° around the occlusion.

The images shown in Fig. 1 highlight the fact that the local intensity in an SEM image can change strongly when a sample is tilted. Such changes in intensity can occur when refocusing the image or as a result of charging effects or changes in relative orientation between the sample surface and the SE detector. In the present study, the reconstruction was successful despite the fact that we did not correct for such artefacts or normalize the intensities in the recorded images. The only pre-processing that was performed was cropping of the images (to the sizes of the dashed rectangles shown in Fig. 1). As noted above, the images should

have enough textural detail for the stitching to be effective. The number of pixels of the images acquired in our experiment is enough to resolve the small particles scattered on the surface of the large nanoparticle. Because a large number of images is required for successful reconstruction, it is always a sensible idea to keep the size of the images (size in pixel and bit resolution) with a values that is enough for resolving the details of the images. We also tried to reconstruct the same dataset after binning the images by a factor of two (down to 668×500 pixels). In this case, the software was unable to perform stitching automatically, probably because of the loss of high resolution detail.

The 3D model of the $LiTi_2(PO_4)_3$ particle shown in Fig. 2a consists of a 3D surface mesh of triangles (Fig. 2b–d). The mesh is an open surface and the final 3D model has a photo-realistic texture, which contains information about the spatial distribution of the recorded image intensity. A UV map was used to describe which parts of the texture should be mapped onto each part of the mesh through an operation that is referred to as unwrapping. The UV map is typically made up of patches, as shown in Fig. 2d. Some of the UV values correspond to the support, some to the particle, while some contain no information about the sample.

Fig. 3 compares the spatial resolution of the texture in the reconstructed 3D model with that in one of the original SEM images. The SEM image shown in Fig. 3a contains streaks due to charging.

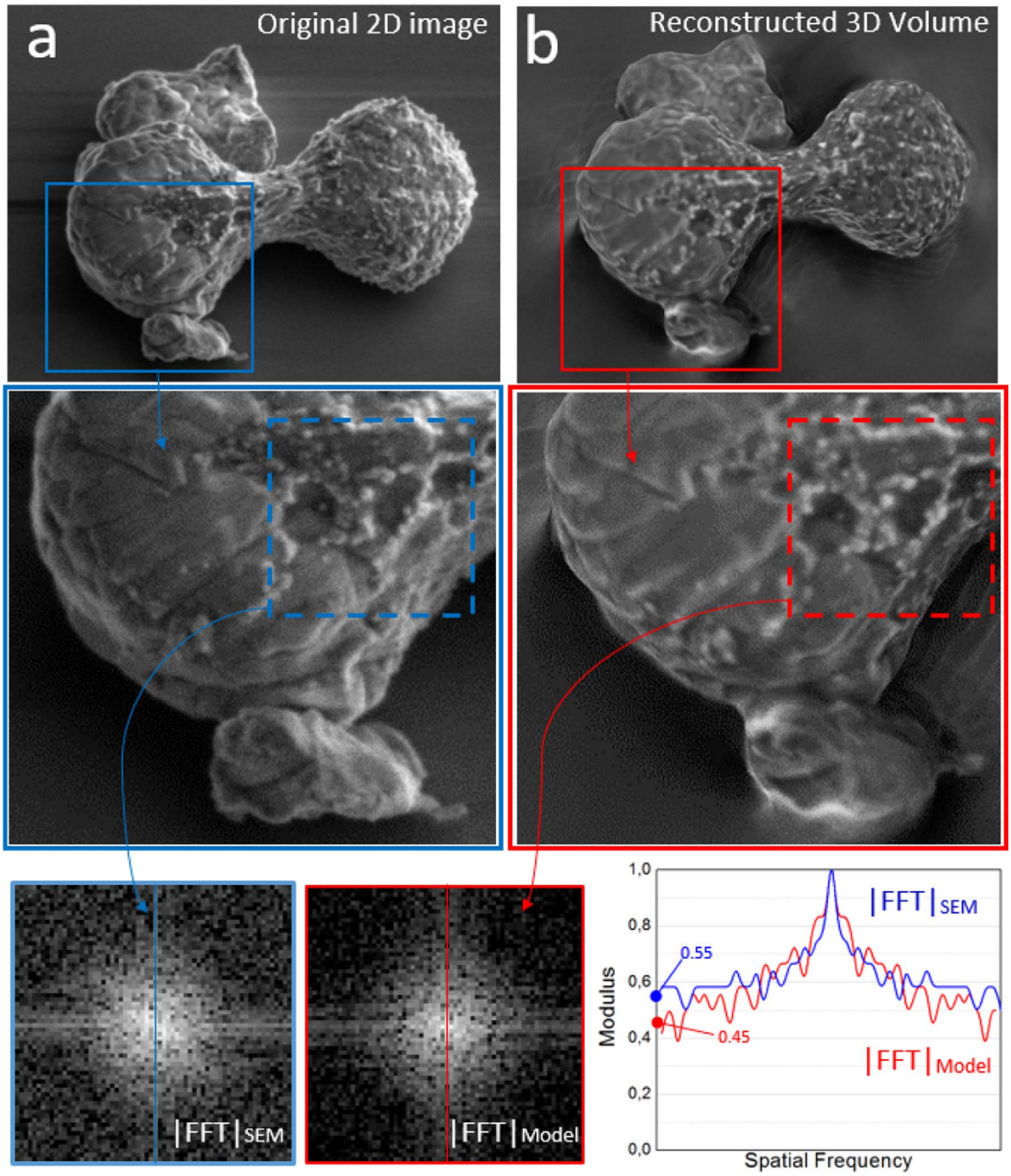

Fig. 3. Comparison of the spatial resolution of (a) an original SEM image and (b) a view of the reconstructed 3D model. The middle row shows magnified regions corresponding to the squares shown in (a) and (b). The 3D reconstruction is slightly more blurred than the original SEM image. The bottom row shows the modulus of the Fourier transform of each of the dashed squares shown in the middle row, alongside line profiles corresponding to the central column of each of the |FFTs|. The line profile generated from the 3D reconstruction decays more rapidly at higher spatial frequencies (by approximately 18% at the cutoff frequency) than that generated from the SEM image.

It is also brighter on the right side of the particle as a result of the location of the SE detector. Fig. 3b shows the 3D model oriented to match the image shown in Fig. 3a. The middle row shows details of the same area in each image, illustrating the fact that the reconstructed model is more blurred. This point is illustrated further in the bottom row of Fig. 3, which shows the modulus of the Fourier transform of each area marked by a dashed square in the middle row. Line profiles generated from the central vertical column in each Fourier transform show that the high spatial frequencies decay faster for the 3D model than for the original SEM image, from about 0.55 to 0.45 (by 18%) at the cutoff frequency (see Fig. 3), corresponding to a slight decrease in spatial resolution in the reconstructed model.

2.1. 2D measurements from UV maps

Eulitz and Reiss [10] did not make use of the possibilities offered by a UV map for texture analysis. The unwrapped UV map is a two-dimensional (2D) image that contains information about the surface of the sample. Therefore, metrology can be applied to it using conventional image processing algorithms. In Fig. 4, the UV map obtained in the present study is used to measure the particle size distribution (PSD) [13] of smaller particles that are distributed over the surface of the $LiTi_2(PO_4)_3$ particle (see middle row in Fig. 3). By using focused ion beam milling and a *slice and view* approach, the smaller secondary phase nanoparticles were identified as titanium oxide and were also found to be present within the primary spindle-like particle [36].

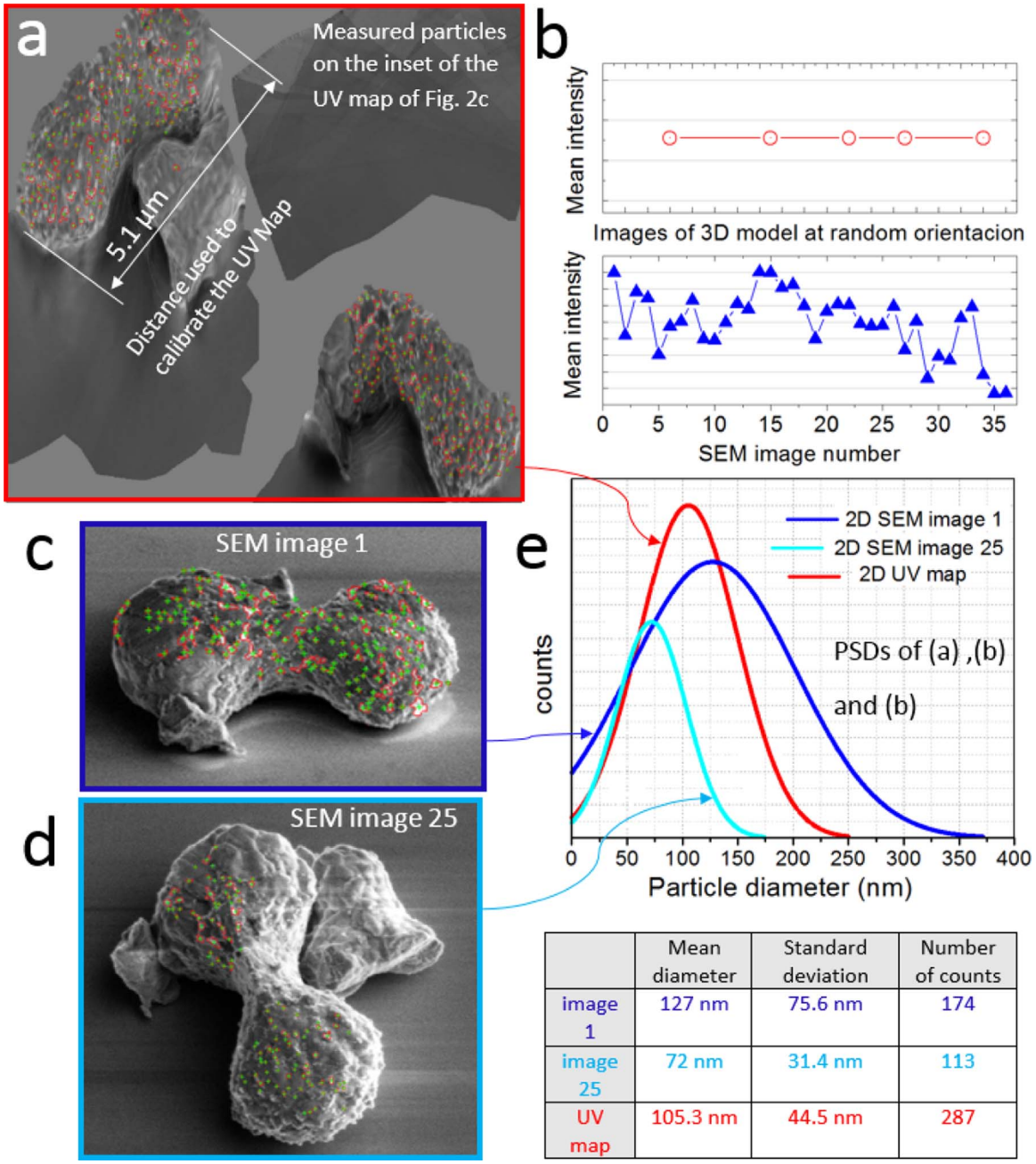

	Mean diameter	Standard deviation	Number of counts
image 1	127 nm	75.6 nm	174
image 25	72 nm	31.4 nm	113
UV map	105.3 nm	44.5 nm	287

Fig. 4. Metrology performed on the UV map of the $LiTi_2(PO_4)_3$ particle. (a) Outlines of nanoparticles on the $LiTi_2(PO_4)_3$ particle used to perform a PSD measurement from the area of the UV map shown in the inset to Fig. 2d. (b) Comparison of the mean intensities of images of the 3D model viewed from five random directions with the mean intensity values of each of the 37 original SEM images used for the reconstruction. (c, d) Outlines of nanoparticles marked on two original SEM images. (e) Histograms and statistical values of PSD measurements performed on both the 3D model and the SEM images shown in (c) and (d).

After calibrating its magnification, the PSD was measured from a part of the UV map that corresponds to the region marked in Fig. 2d. The fitted outlines of the particles are marked in Fig. 4a. Fig. 4c and d shows corresponding segmented PSDs determined from two of the original SEM images. Fig. 4e compares histograms and statistical measurements of the PSDs determined from both the UV map and the SEM images. Significantly, the PSD measurements vary between the two SEM images. In contrast, there are several advantages to using the UV map for metrology. First, it has a more uniform background than the original SEM images because photogrammetric reconstruction averages local intensities over the complete series of images used for reconstruction. The greater uniformity of the contrast facilitates image processing operations such as thresholding. This difference in the uniformity of the contrast can be seen between the SEM image shown in Fig. 3a and the 3D model shown in Fig. 3b. The SEM image shows stronger changes in intensity between different areas. In addition, the sample appears to be illuminated from the right side. This apparent directionality of illumination is typical of SEM images, but is almost absent in the photogrammetric reconstruction shown in Fig. 3b. Fig. 4b compares the mean intensities of images of the 3D model viewed from five random directions with the mean intensity values of each of the 37 original SEM images used for the reconstruction. The average intensity is constant for the views of the 3D model, whereas it varies between the SEM images. Second, the contrast of the small particles on the support is higher in the 3D model (and in the corresponding UV map). This difference is also apparent between Fig. 3a and b. A further advantage of using the UV map for metrology is that it is an unwrapped version of a 3D surface, meaning that a measurement is more representative of the entire sample surface, when compared with that from an individual SEM image, which shows only part of the surface. However, a disadvantage of using the UV map is that the spatial resolution of the 3D model is lower, meaning that some of the smaller particles that are too close to each other can appear to be "coalesced". As a result, care is needed to ensure that a PSD determined from a UV map does not contain artefacts.

2.2. 3D measurements of geometry

We used the *Meshlab* freeware [22] to measure geometrical parameters from the 3D model. First, the parts of the mesh corresponding to the support were deleted manually. Second, in order to perform accurate geometrical measurements, it was ensured that the mesh was "watertight", i.e., closed, by exporting the file in .x3d format and processing it using the program *Netfabb Basic* [24] (see the Methods section). This processing step flattens the side of the particle that was in contact with the support. The model was then loaded into *Meshlab* software [22], its magnification was calibrated (see Fig. 5a and b) and geometrical parameters describing the object (summarized in the Table in Fig. 5c) were measured. It should be noted that the underside of the particle is not detectable using SEM and cannot be reconstructed by use of photogrammetry, thereby introducing an error when the total surface of the particle is

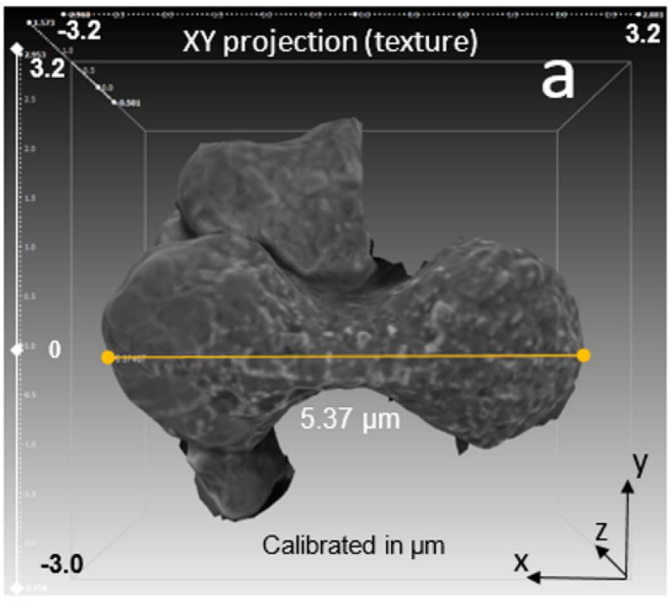

c

Geometrical measures	
Mesh volume	16.18 µm³
Mesh surface	54.19 µm²
Thin shell barycenter	(-0.39, 0.34 ,0.45)
Center of mass	(-0.53, 0.33, 0.54)
Inertia Tensor	$\begin{vmatrix} 16.95 & 2.79 & -1.80 \\ 2.79 & 36.62 & 1.39 \\ -1.80 & 1.39 & 47.70 \end{vmatrix}$
Principal axes	$\begin{vmatrix} 0.99 & -0.14 & 0.06 \\ 0.15 & 0.98 & -0.10 \\ 0.05 & -0.11 & -0.99 \end{vmatrix}$
Axis momenta	(16.43 36.89 47.94)

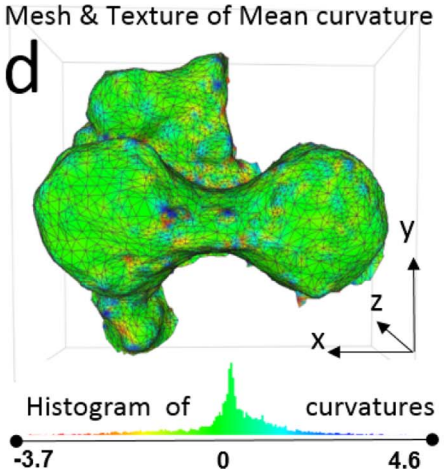

Fig. 5. Processing and analysis of the 3D model of the $LiTi_2(PO_4)_3$ particle. (a, b) Calibrated views of the particle viewed perpendicular to the XY and XZ planes. The support was removed using the program *Meshlab freeware* [22], while the lower surface was closed (repaired) using the program *Netfabb Basic* [24]. (c) Geometrical measurements of the particle determined using *Meshlab software* [22]. (d) Visualization of the mesh surface of the particle viewed perpendicular to the XY plane, showing variations in its mean curvature (using colors) over the range −3.7 to 4.6. (For interpretation of the references to color in this figure, the reader is referred to the web version of this article.)

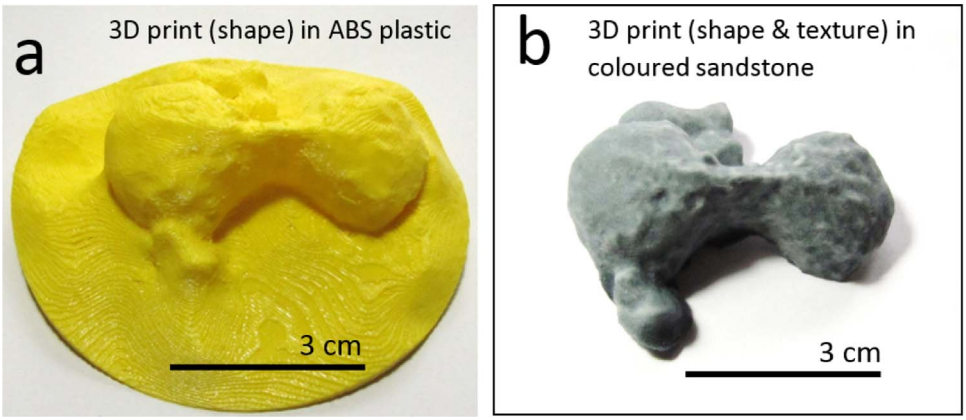

Fig. 6. (a) Printed plastic model of the of the $LiTi_2(PO_4)_3$ particle and its support. (b) Printed model of the particle, including its surface texture, in colored sandstone. (For interpretation of the references to color in this figure legend, the reader is referred to the web version of this article.)

computed. Fig. 5d shows the 3D model with a colored texture, in which different colors represent variations in the measured mean curvature of the surface. The mean curvature is defined as half of the sum of the principal curvatures and has units of inverse length.

2.3. 3D printing

3D printing can be used to display and disseminate 3D data [10,17,19]. Fig. 6 shows a model of the $LiTi_2(PO_4)_3$ particle fabricated using 3D printing. In order to prepare the file for printing, pre-processing was required, as described in the Methods section. Fig. 6a shows a model of the supported particle printed in ABS plastic after the model was thickened using the software *Cura* [8]. Fig. 6b shows a model of the particle after removing the support and correcting it so that it was "watertight", printed in sandstone color using an online printing service that allows not only shape but also texture to be reproduced (grayscale tonality). It should be noted that the resolution and contrast of the printed model in Fig. 6b are slightly poorer than that of the digital reconstruction.

3. Summary and conclusions

The methodology that we describe here for 3D reconstruction,

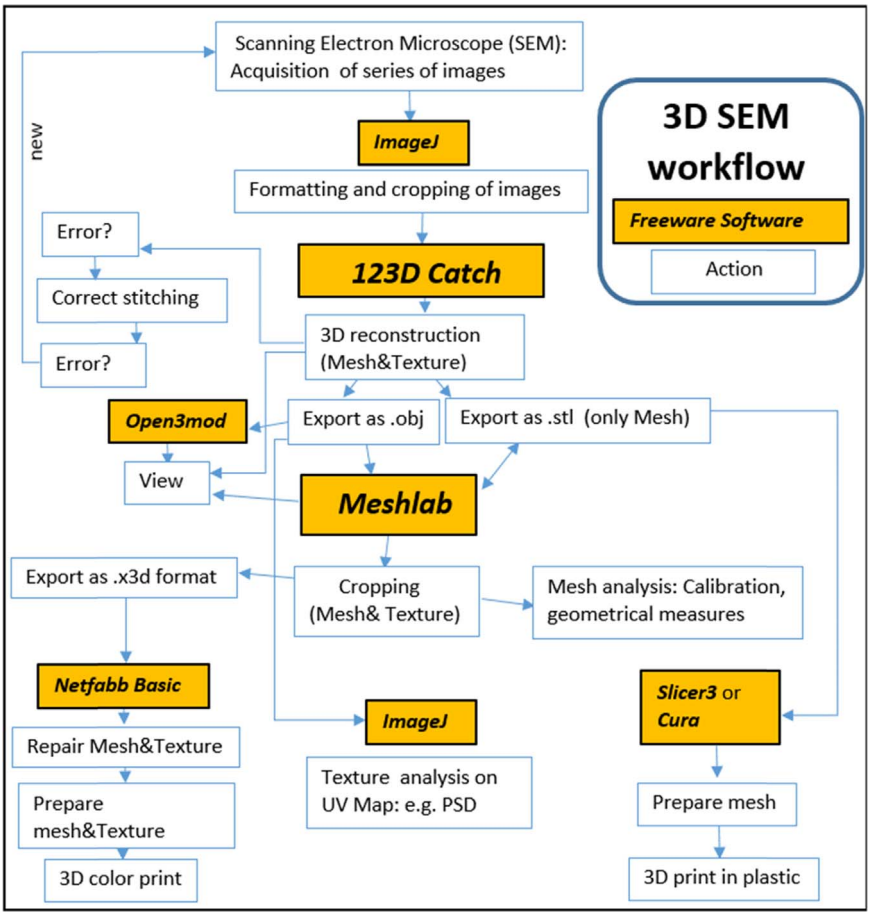

Fig. 7. Summary of the freeware and processing steps used in the present study.

analysis and printing of the shape and texture of a $LiTi_2(PO_4)_3$ particle using SEM is summarized in Fig. 7. The approach does not require special hardware. In the present study, it took one hour to acquire the images and less than one hour to perform automatic 3D reconstruction. Moreover, the software required for reconstruction is free, on the cloud and available to anyone with an internet connection. Furthermore, its simplicity results in a rapid learning curve. However, there is little room for optimization of the reconstruction parameters due to the "black box" nature of the software used. In the work presented here, open file formats (.obj and .x3d) and freeware viewers were used. Because the UV map of the 3D model is saved as a separate.jpeg image in .obj format, we have shown that it can be used directly for analyzing the information contained on a 3D surface in a simple manner using any image processing algorithm, especially for metrological measurements. In terms of size, while a single SEM image occupies 1.28 Mb, the .obj file, which contains full 3D information, occupies 1.67 Mb (1.17 Mb, 396 bytes and 518 kb for the .obj, .mtl and .jpeg files, respectively). The acquisition of a series of images can easily be automated in most modern SEMs by using software to control the tilt and rotation of the sample holder. In addition, other signals that contain compositional information, such as X-rays and backscattered electrons, can also be used separately or combined for photogrammetric reconstruction.

Methods

The spindle-like $LiTi_2(PO_4)_3$ particle studied in this paper was prepared by a solvothermal route that allows particles of homogeneous size and shape to be produced [36]. A dry powder of $LiTi_2(PO_4)_3$ particles was deposited onto an SEM pin mount. The sample was scanned until an isolated particle was found. A series of images was recorded in an FEI Helios NanoLab field emission gun (FEG) SEM operated in SE mode using an Everhart-Thornley detector (ETD). The microscope has a stage with an α-tilt range of $-3°$ to 60°. The SEM was operated at a working distance (WD) of 4 mm with a horizontal field width (HFW) of 15.9 μm. The accelerating voltage was set to a low value of 2 kV to reduce electrostatic charging of the sample. Images with 1536×1092 pixels and a pixel size of 0.01 μm were initially saved in .tif format with 3 channels of 8 bits (24 bit depth), resulting in a total file size of 4.81 Mb.

Each image was pre-processed using *ImageJ* software [18] in order to reduce it to one grey scale channel (Image- > Colors- > Split Channels), cropped to a size of 1337×1000 pixels (Select ROI, Image- > Crop) and saved in .tif format with a size of 1.28 Mb.

The entire dataset of 37 images was loaded into *123D Catch* (freeware from *Autodesk*) [1]. 3D reconstruction of the particle surface was then performed online in the cloud. The software can fail during reconstruction due to poor quality data or internal software crashes. In the event of problems with stitching the images, the software has an interactive tool that can be used to mark common points between consecutive images manually. However, based on our experience it is always better to acquire a good tilt series with enough images, sufficient overlap between images, enough intensity features and no occlusions. Once the reconstruction has been completed, the same software can be used offline to explore the 3D file, to view the model from different directions and to zoom in and out. Alternatives involve trying to reconstruct the dataset again or acquiring a new dataset. The software permits a model to be reconstructed using "high quality" mesh resolution, with a greater number of faces and vertices at the cost of longer computing time. Nevertheless, the 3D model in the present study was reconstructed using a standard mesh resolution.

The 3D model can be exported and downloaded using one of several open file formats. As explained in the text, the 3D model is a mesh with a texture. The surface model without texture can be saved as a stereolithography (.stl) file, which can subsequently be processed for 3D printing. In the present paper, the 3D model was exported and saved in .obj format, which records information about both the mesh and the surface texture. The .obj format saves three files: one with a filename ending *.obj describing the 3D mesh, one with a filename ending *.mtl containing information for 3D visualization and the name of the UV map and a *.jpeg image that contains the texture.

3D files were viewed using *Open3mod* software [25], which provides the basic functionality to open .obj files and explore a 3D model (rotating and zooming). Alternatively, *MeshLab* freeware [22] (version 1.3.3) could be used to manipulate and analyze the .obj file and other file formats.

In order to perform accurate geometrical measurements, the particle was segmented from the support by deleting all of the triangles of the mesh around it using *MeshLab* (Select Faces in a rectangular region- > Delete set of selected faces). The open mesh was exported from *MeshLab* in .x3d format. The .x3d file could then be imported into *Netfabb Basic* (version 6.4) [24], free software that can be used to check, correct errors and close meshes.

The final model was re-imported into *MeshLab* and calibrated in units of μm (*Meshlab*- > Filters- > Normals, Curvatures and Orientation- > Transform: Scale). The curvature shown in Fig. 5 was defined (*Meshlab* > Filters > Color Creation and Processing > Colorize by curvature (APSS)) and the option Mean Curvature was selected. Different definitions of curvatures could be chosen, including Mean, Gauss, K1, K2 and ApproxMean. The geometrical measures presented in the Table in Fig. 5 could then be calculated (*Meshlab*- > Filters- > Quality Measures and Computations- > Compute Geometric Measures).

For 3D printing in plastic (Fig. 6a), the 3D model was exported from *Meshlab* in .stl format, which is the most common file format for defining 3D meshes. Before printing, the .stl mesh was corrected for imperfections and some material was added to it to increase the rigidity of the model, as the initial mesh has no thickness. These steps could be performed using open source programs such as *Cura 3d* [8] and *Slice3r* [32]. Both programs also generate G-Codes, which the electronics of a 3D printer uses to move and deposit material. In order to print a 3D model that includes grayscale texture, an online 3D printing service was used to print the model in sandstone with a color option. The mesh and texture then had to be "watertight", i.e., the mesh had to be closed and without holes. Such defects were corrected by exporting the 3D model in .x3d format using *Meshlab*, importing the .x3d file into *Netfabb Basic* (version 6.4) to check and correct errors in the mesh and then uploading the corrected model in .x3d format to the webpage of *Shapeways* (Eindhoven, The Netherlands). This online service provides tools for final revision of the suitability of the model for printing, as well as for scaling it to a desired size.

Additional information

An .obj file of the 3D model and a video describing the workflow can be found online at http://dx.doi.org/10.1016/j.ultramic.2016.07.006.

Acknowledgments

Financial support from the European Union Seventh Framework Programme under Grant Agreement 312483 – ESTEEM2 (Integrated Infrastructure Initiative – I3) is acknowledged. The FEI

Helios 460 F1 used in this work was funded by the Bundesministerium für Bildung und Forschung (BMBF) under project SABLE 03EK3543.

Appendix A. Supporting information

Supplementary data associated with this article can be found in the online version at http://dx.doi.org/10.1016/j.ultramic.2016.07.006.

References

[1] 123D Catch from Autodesk. ⟨http://www.123dapp.com/catch⟩.
[2] B.G. Bang, F.B. Bang, Graphic reconstruction of the third dimension from serial electron microphotographs, J. Ultrastruct. Res. 1 (1957) 138–146.
[3] P. Bariani, L. De Chiffre, H.N. Hansen, A. Horsewell, Investigation on the traceability of three dimensional scanning electron microscope measurements based on the stereo-pair technique, Precis. Eng. 29 (2005) 219–228.
[4] S.P. Bemis, S. Micklethwaite, D. Turner, M.R. James, S. Akciz, S.T.T. Thiele, H. A. Bangash, Ground-based and UAV-based photogrammetry: a multi-scale, high-resolution mapping tool for structural geology and paleoseismology, J. Struct. Geol. 69 (2014) 163–178.
[5] L. Carli, G. Genta, A. Cantatore, G. Barbato, L. De Chiffre, R. Levi, Uncertainty evaluation for three-dimensional scanning electron microscope reconstructions based on the stereo-pair technique, Meas. Sci. Technol. 22 (2011) 035103.
[6] L. Carli, 3D-SEM Metrology for Coordinate Measurements at the Nanometer Scale (Ph.D. Thesis), Department of Mechanical Engineering, Technical University of Denmark, Denmark, 2010.
[7] R.A. Crowther, D.J. de Rosier, A. Klug, The reconstruction of a three-dimensional structure from projections and its application to electron microscopy, Proc. R. Soc. Lond. A 319 (1970) 317–340.
[8] Cura 3d. ⟨https://ultimaker.com/en/products/cura-software⟩.
[9] W. Denk, H. Horstmann, Serial block-face scanning electron microscopy to reconstruct three-dimensional tissue nanostructure, PLoS Biol. 2 (11) (2004) 1900–1909, e329.
[10] M. Eulitz, G. Reiss, 3D reconstruction of SEM images by use of optical photogrammetry software, J. Struct. Biol. 191 (2015) 190–196.
[11] P.L. Falkingham, Acquisition of high resolution 3D models using free, open source, photogrammetric software, Palaeontol. Electron. 15 (1) (2012) 15.
[12] C.A. García-Negrete, M.J. de Haro, J. Blasco, M. Soto, A. Fernández, STEM-in-SEM high resolution imaging of gold nanoparticles and bivalve tissues in bioaccumulation experiments, Analyst 140 (9) (2015) 3082–3089.
[13] L.C. Gontard, D. Ozkaya, R.E. Dunin-Borkowski, A simple algorithm for measuring particle size distributions on an uneven background from TEM images, Ultramicroscopy 111 (2011) 101–106.
[14] L.C. Gontard, J.R. Jinschek, H. Ou, J. Verbeeck, R.E. Dunin-Borkowski, Three-dimensional fabrication and characterisation of core–shell nanocolumns using electron beam patterning of Ge-doped SiO_2, Appl. Phys. Lett. 100 (2012) 263113.
[15] O. Guise, C. Strom, N. Preschilla, STEM-in-SEM method for morphology analysis of polymer systems, Polymer 52 (5) (2011) 1278–1285.
[16] H.N. Hansen, K. Carneiro, H. Haitjema, L. De Chiffre, Dimensional micro and nano metrology, CIRP Ann. - Manuf. Technol. 55 (2) (2006) 721–743.
[17] L. Hughes, 3D printing for biological electron microscopy July-Aug, Microsc. Anal. (2015) 14–17.
[18] ImageJ. ⟨http://imagej.nih.gov/ij/⟩.
[19] N. Jones, Three-dimensional printers are opening up new worlds to research, Nature 487 (2012) 23.
[20] P. Jornsanoh, G. Thollet, J. Ferreira, K. Masenelli-Varlot, C. Gauthier, A. Bogner, Electron tomography combining ESEM and STEM: a new 3D imaging technique, Ultramicroscopy 111 (2011) 1247–1254.
[21] A.J. Koster, U. Ziese, A.J. Verkleij, A.H. Janssen, K.P. de Jong, Three-dimensional transmission electron microscopy: a novel imaging and characterization technique with nanometer scale resolution for materials science, J. Phys. Chem. B 104 (2000) 9368–9370.
[22] Meshlab. ⟨http://meshlab.sourceforge.net/⟩ and online version ⟨http://www.meshlabjs.net/⟩.
[23] P.A. Midgley, R.E. Dunin-Borkowski, Electron tomography and holography in materials science, Nat. Mater. 8 (2009) 271–280.
[24] Nettfab. ⟨http://www.netfabb.com/basic.php⟩.
[25] Open3mod. ⟨http://www.open3mod.com/⟩ by Alexander Gessler.
[26] C.J. Peddie, L.M. Collinson, Exploring the third dimension: Volume electron microscopy comes of age, Micron 61 (2014) 9–19.
[27] P. Penczek, M. Radermacher, J. Frank, Three-dimensional reconstruction of single particles embedded in ice, Ultramicroscopy 40 (1992) 33–53.
[28] G. Piazzesi, Photogrammetry with the scanning electron microscope, J. Phys. E: Sci. Instrum. 6 (4) (1973) 392.
[29] L. Repetto, R. Buzio, C. Denurchis, G. Firpo, E. Piano, U. Valbusa, Fast three-dimensional nanoscale metrology in dual-beam FIB-SEM instrumentation, Ultramicroscopy 109 (2009) 1338–1342.
[30] M. Sailer, K. Höhn, S. Lück, V. Schmidt, M. Beil, P. Walther, Novel electron tomographic methods to study the morphology of keratin filament networks, Microsc. Microanal. 16 (2010) 462–471.
[31] M. Schubert, A. Gleichmann, M. Hemmleb, J. Albertz, J.M. Kijhler, Determination of the height of a microstructure sample by a SEM with a conventional and a digital photogrammetric method, Ultramicroscopy 63 (1996) 57–64.
[32] Slice3r. ⟨http://slic3r.org/⟩.
[33] G.E. Soto, S.J. Young, M.E. Martone, T.J. Deerinck, S. Lamont, B.O. Carragher, K. Hama, M.H. Ellisam, Serial section electron tomography: a method for three-dimensional reconstruction of large structures, Neuroimage 1 (1994) 230–243.
[34] J. Stampfl, S. Scherer, M. Gruber, O. Kolednik, Reconstruction of surface topographies by scanning electron microscopy for application in fracture research, Appl. Phys. A 63 (4) (1996) 341–346.
[35] VisualFSM. ⟨http://ccwu.me/vsfm/⟩.
[36] S. Yu, H. Tempel, R. Schierholz, Ö. Aslanbas, X. Gao, J. Mertens, L.G.J. deHaart, H. Kungl, R-A. Eichel, $LiTi_2(PO_4)_3$ anode material with a spindle-like morphology for batteries with high rate capability and improved cycle life, Chem ElectroChem 3 (7) (2016) 1157–1169.
[37] M. Weyland, Two and Three-dimensional Nanoscale Analysis: New Techniques and Applications (Ph.D. Thesis), University of Cambridge, United Kingdom, 2002.
[38] K.W. Wong, Mathematical formulation and digital analysis in close-range photogrammetry, Photogramm. Eng. Remote Sens. 44 (1975) 11.